Well Hydraulics in a Two-Zone Aquifer under Ambient Flow: Analytical Study

Ali Mahdavi [*,1], Ying-Fan Lin [2]

1. Department of Civil Engineering, Arak University, Arak, Iran.
2. Department of Civil Engineering, Chung Yuan Christian University, Taoyuan, Taiwan.

***Corresponding Author:**
Ali Mahdavi

Email: a-mahdavi@araku.ac.ir
Received: 2026.07.20
Accepted: 2026.11.05
J. Hydraul. Struct., 2027;13(2):44-66
DOI: 10.22055/jhs.2026.52699.1391

ABSTRACT

Pump-and-treat performance depends on capture zones around pumping wells. In low-permeability aquifers, constant-rate models often misrepresent flow. This study develops a mathematical model for groundwater flow under constant-head pumping to delineate the well capture zone. The model includes wellbore skin and the regional hydraulic gradient. Closed-form expressions for drawdown and stream function support flow-net analysis in the skin and formation zones. Adaptive finite-element simulations validate the solutions. Results identify a downstream stagnation point, define capture-zone envelopes, and quantify transit time as functions of ambient-flow strength and aquifer contrasts. Wellbore flow increases only when skin permeability exceeds formation permeability; when formation conductivity exceeds skin conductivity, skin-radius effects become negligible. Dimensionless transit time decreases from ~90,000 to ~30,000 as ambient-flow strength increases from 0.01 to 0.03, indicating regional gradients accelerate transport, while heterogeneity exerts a weaker influence. A least-squares parameter-estimation procedure recovers hydraulic conductivity and ambient-flow velocity. The framework supports design and evaluation of constant-head pump-and-treat systems in low-permeability aquifers.

KEYWORDS

Analytical groundwater modeling; Aquifer heterogeneity; Capture zone delineation; constant-head pumping; Two-zone groundwater flow.

1. Introduction

Groundwater serves as an indispensable resource, particularly in regions where surface water availability is either insufficient or highly unpredictable. Its significance has driven extensive research aimed at optimizing exploration, safeguarding its quality, and implementing sustainable management strategies [1,2]. Recent studies emphasize the growing challenges posed by urbanization, industrial activities, and climate change, which contribute to groundwater contamination through pollutants such as toxic metals, hydrocarbons, pesticides, and emerging contaminants like microplastics and nanoparticles [3]. Efforts to protect groundwater quality are crucial not only for environmental conservation but also for ensuring public health and long-term sustainability. Advanced geochemical and geospatial techniques are being employed to monitor and assess contamination risks, while innovative remediation strategies, including bioremediation and new materials for sustainable purification, are gaining traction.

Additionally, policy frameworks and regulatory measures are evolving to address the complexities of groundwater protection, balancing industrial benefits with environmental safety [4].

Building on these protection needs, current remediation practice relies on hydraulic containment strategies. Pump-and-treat continues to be a widely employed technique for the remediation of contaminated aquifers, demonstrating its effectiveness in mitigating groundwater pollution [5]. This method entails the extraction of polluted groundwater, followed by treatment processes designed to remove a range of contaminants, including organic compounds, heavy metals, and emerging pollutants. Depending on site-specific conditions and regulatory requirements, the treated water may either be safely discharged into surface water systems or reinjected into the aquifer to support groundwater replenishment and maintain hydrological balance. Advances in treatment technologies, such as enhanced filtration systems, chemical oxidation, and bioremediation, continue to improve the efficiency and sustainability of pump-and-treat, reinforcing its role as a cornerstone in groundwater management strategies [6].

Transitioning to capture-zone delineation clarifies how containment outcomes depend on flow geometry. Central to the efficacy of this method is the concept of capture zones - areas around pumping wells from which water and dissolved contaminants are extracted over a specific period [7,8]. Accurate delineation of these zones is crucial for predicting the spatial extent of groundwater extraction and optimizing the placement of extraction wells for efficient contaminant removal. Capture zone envelope models have evolved to account for complex hydrogeologic conditions, including heterogeneous and anisotropic aquifer properties, multiple wells, variable pumping rates, and the effects of advection, dispersion, and chemical reactions on contaminant transport [9,10,11]. These include analytical solutions, numerical simulations, and particle tracking techniques. However, existing approaches for developing capture zone envelopes have predominantly focused on constant-rate pumping wells [12,13]. Direct analytical developments for constant-head pumping are comparatively limited. Existing capture-zone and pumping-test formulations largely assume constant-rate extraction, leaving practitioners without an analytical counterpart for constant-head containment where well hydraulics are governed by maintained drawdown.

A significant challenge arises when groundwater contamination is located in low-permeability regions of an aquifer [14]. In such cases, pumping rates must be carefully controlled to avoid overdraft problems in shallow aquifers [15] and over-extraction from the pumping well in low-permeability formations. To address these challenges, constant-head pumping has emerged as an effective alternative and is gaining traction in hydrogeological applications [16,17,18]. This technique maintains a constant water level or pressure in a well during water extraction, offering a steady supply of water - a particularly advantageous feature in low-permeability aquifers. By implementing this approach, contamination plumes can be efficiently contained, inhibiting further seepage into the aquifer. The withdrawn water can then undergo treatment to remove pollutants before reuse, discharge, or re-injection.

To operationalize constant-head management, constant pumping tests play a vital role in estimating the hydraulic properties of aquifers and assessing their capacity to sustain water extraction. By maintaining a steady flow rate or hydraulic head, these tests provide valuable data on parameters such as permeability, transmissivity, and storativity, which are essential for groundwater modeling and management [19]. Additionally, they help evaluate the interaction between the well and the surrounding formation, ensuring efficient design and placement of wells. Constant pumping tests are particularly

important in regions with limited water resources, as they enable informed decisions for sustainable groundwater utilization and protection. Their significance extends to contaminant transport studies, allowing for the prediction and optimization of remediation strategies. Emerging research highlights the integration of pumping test data with geophysical and remote sensing techniques to improve contamination assessments and mitigation efforts [20].

Despite the growing use of constant-head pumping, capture zone envelopes tailored for this method remain insufficiently investigated. This study develops a mathematical model of groundwater flow induced by constant-head pumping to address this gap. The model accounts for wellbore skin and background flow driven by natural hydraulic gradients, providing a comprehensive representation of field conditions. Previous studies identified the influence of regional groundwater flow on capture zones under variable climatic and anthropogenic conditions, emphasizing their sensitivity to recharge and withdrawal rates [11,21]. Groundwater transit time governs contaminant migration by determining the residence period of solutes in the aquifer. Although analytical solutions exist for homogeneous systems, estimating transit time in heterogeneous media under pumping remains challenging. Variations in permeability and localized hydraulic responses hinder development of a generalized analytical model [22,23]. This study introduces a closed-form analytical solution that computes the travel time of a fluid particle from the radius of influence to the wellbore while incorporating aquifer heterogeneity within the skin zone. An analytical framework is also established to estimate parameters representing ambient flow and heterogeneity from observed drawdowns. This hydrogeological characterization improves understanding of groundwater movement, hydraulic properties, stratigraphic structure, and flow rates. Methodologically, the derivation applies potential theory; the Cauchy-Riemann equations ensure conjugacy between hydraulic head and stream function, and boundary-condition expansions yield unknown constants through Fourier coefficients.

To summarize, the novelty of the present study lies in the following contributions: (i) development of a closed-form analytical solution for steady-state groundwater flow induced by a constant-head pumping well in a two-zone confined aquifer with unidirectional ambient flow and distinct hydraulic conductivities in the skin and formation zones; (ii) analytical characterization of the flow field through the corresponding stream function, including the effects of hydraulic heterogeneity on streamline refraction and capture-zone boundaries; (iii) analytical examination of the effects of ambient-flow velocity, heterogeneity ratio, and skin-zone extent on drawdown, well discharge, stagnation-point location, capture-zone geometry, and groundwater transit time; and (iv) development of an inverse parameter-estimation framework for determining the hydraulic conductivity of the skin zone and ambient-flow velocity from drawdown observations, together with an assessment of its robustness to observational noise and monitoring-well configuration.

2. Model Setup

Figure 1 depicts a schematic diagram of a steady-state flow model in a radial two-zone confined aquifer. This flow is induced by constant-head pumping with constant wellbore drawdown of s_w [L] and unidirectional ambient flow with constant Darcian velocity of U [LT^{-1}] at a fully penetrating well with a finite radius of r_w [L]. The aquifer is divided into two distinct zones with different hydraulic properties: an inner skin zone and an outer formation zone. These zones are denoted by subscripts 1 and 2, respectively. The drawdowns of the two zones are represented as s_1 [L] for the inner skin zone and s_2 [L] for the outer formation zone. The hydraulic

conductivities are K_1 [LT^{-1}] in the skin zone and K_2 [LT^{-1}] in the formation zone; K_i are assumed isotropic in r- and θ-directions. The skin zone extends from $r = r_w$ to $r = r_s$; the formation zone extends from $r = r_s$ to a finite outer radius R [L]. We use coordinates (r, θ) centered at the well, with $0 \le \theta < 2\pi$. Physically, the ambient Darcian velocity U [LT^{-1}] represents the far-field specific discharge induced by a regional hydraulic gradient; in the formation zone $U = K_2 \nabla s$, and we define $\theta = 0$ along the ambient-flow direction.

The drawdown equation can be expressed in dimensionless form by introducing dimensionless variables and parameters $s_{i,D} = s_i/s_w$, $r_D = r/r_w$, $r_{s,D} = r_s/r_w$, $R_D = R/r_w$, $U_D = Ur_w/(K_2 s_w)$, and $\kappa = K_2/K_1$; that is

$$\frac{\partial^2 s_{i,D}}{\partial r_D^2} + \frac{1}{r_D}\frac{\partial s_{i,D}}{\partial r_D} + \frac{1}{r_D^2}\frac{\partial^2 s_{i,D}}{\partial \theta^2} = 0,\ i = 1 \text{ and } 2 \quad (1)$$

Equation (1) holds in zone 1 for $1 \le r_D < r_{s,D}$ and in zone 2 for $r_{s,D} \le r_D < R_D$.

The boundary condition at the wellbore surface for describing the constant drawdown pumping can be expressed as

$$s_{1,D}\big|_{r_D=1} = 1 \quad (2)$$

At the interface between the skin zone and formation zone, two continuity requirements are imposed. The associated conditions at this interface are as follows:

$$s_{1,D}\big|_{r_D=r_{s,D}} = s_{2,D}\big|_{r,D=r_{s,D}} \quad (3)$$

and

$$\frac{\partial s_{1,D}}{\partial r_D}\bigg|_{r_D=r_{s,D}} = \kappa \frac{\partial s_{2,D}}{\partial r_D}\bigg|_{r_D=r_{s,D}} \quad (4)$$

The continuity conditions at the interface in the θ direction should be satisfied as follows:

$$s_{i,D}\big|_{\theta=0} = s_{i,D}\big|_{\theta=2\pi} \quad (5)$$

and

$$\frac{\partial s_{i,D}}{\partial \theta}\bigg|_{\theta=0} = \frac{\partial s_{i,D}}{\partial \theta}\bigg|_{\theta=2\pi} \quad (6)$$

The formation zone is subjected to a unidirectional ambient flow characterized by Darcian velocity of U. This flow is considered in the remote boundary condition as $s_2|_{r=R} = UR\cos\theta/K_2$ The dimensionless form of this boundary condition reads

$$s_{2,D}\big|_{r_D=R_D} = U_D R_D \cos\theta \quad (7)$$

where $U_D = Ur_W/(K_2 s_W)$. The radial distance far from the pumping is influenced solely by the background hydraulic gradient, as indicated by equation (7). Such conditions frequently occur in classical fluid mechanics when specifying free-stream potentials at the remote end of the flow system. For reference, $\kappa = K_2/K_1$ is the hydraulic conductivity ratio; $\kappa = 1$ reduces the model to a homogeneous aquifer.

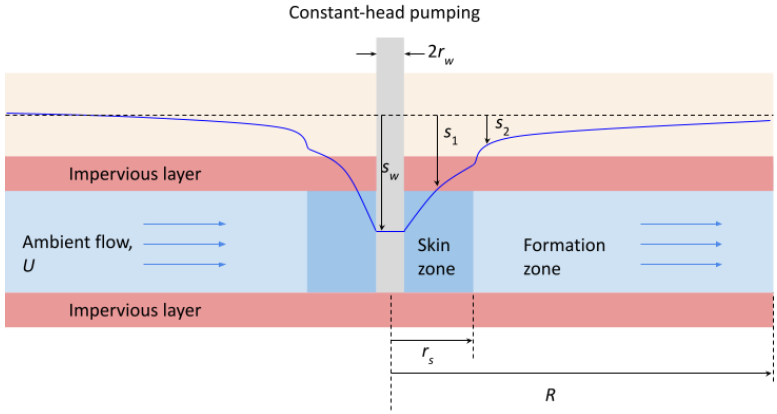


Fig. 1 Schematic diagram of a constant-head pumping conducted in a two-zone confined aquifer subject to ambient flow.

3. Analytical Solutions of Drawdown Distribution

The general solution of model Eq. (1) satisfying Eqs. (5) and (6) can be expressed in the following form based on the method of separation of variables:

$$\begin{aligned} s_{i,D} = A_{i,0} + B_{i,0}\ln r_D \\ + \sum_{n=1}^{\infty}\left(A_{i,n}r_D^{n}\right. \\ \left. + B_{i,n}r_D^{-n}\right)\cos n\theta \\ + \sum_{n=1}^{\infty}\left(C_{i,n}r_D^{n}\right. \\ \left. + D_{i,n}r_D^{-n}\right)\sin n\theta \end{aligned} \tag{8}$$

The unknown coefficients $A_{i,0}$, $B_{i,0}$, $A_{i,n}$, $B_{i,n}$, $C_{i,n}$ and $D_{i,n}$ in Eq. (8) are determined in accordance with the boundary conditions (Appendix A) and the results are listed in Table 1. Because the well boundary (Eq. (2)) is axisymmetric (constant) and the remote boundary (Eq. (7)) is proportional to $\cos\theta$ (an even function), only cosine terms are forced; all sine terms vanish by symmetry. Moreover, a uniform far-field perturbation excites only the $n = 1$ angular mode; higher harmonics ($n \geq 2$) are not required by the boundary data. Consequently, the general representation in Eq. (8) degenerates to a cosine series with only one term associated with $n = 1$. Physically, this reduction corresponds to the superposition of an axisymmetric pumping potential ($n = 0$ terms) and a dipole-like response to uniform ambient flow ($n = 1$ cosine term). Therefore, all the remaining coefficients must disappear. The drawdown distribution can then be expressed in closed-form as follows:

$$\begin{aligned} s_{i,D} = A_{i,0} + B_{i,0}\ln r_D \\ + \left(A_{i,1}r_D\right. \\ \left. + \frac{B_{i,1}}{r_D}\right)\cos\theta \end{aligned} \tag{9}$$

Eq. (9) consists of three terms on the right-hand side. The first two terms, $A_{i,0} + B_{i,0}\ln r_D$, account for the well contribution to the model drawdown response. The last term, $\left(A_{i,1}r_D + B_{i,1}/r_D\right)\cos\theta$, represents the influence of ambient flow. By leveraging the uniqueness property of Fourier coefficients, a system of eight linearly independent equations is established. This system enables the determination of the coefficient values in Eq. (9). It is easy to verify that $\partial s_{2.D}/\partial r_D = U_D\cos\theta$ at $r_D = R_D$ when $R_D \to \infty$.

3.1. Derivation of Stream Functions

A crucial aspect of analyzing groundwater flow dynamics involves transforming the analytical model for hydraulic head into a system of equations based on a stream function. This formulation is advantageous for achieving precise streamlines compared to the drawdown (or potential function) formulation. The stream function method helps track groundwater flow paths through specific locations within nested groundwater flow systems. This approach is gaining recognition when addressing groundwater contamination challenges and conducting groundwater age dating studies [22].

Once the drawdown solutions are derived, the stream functions can then be obtained for predicting the flow streamlines. The Cauchy-Riemann equations that connect the stream function Ψ_i to drawdown can be written in polar coordinates as

$$\frac{\partial\Psi_i}{\partial r} = \frac{K_i}{r}\frac{\partial s_i}{\partial\theta} \tag{10}$$

$$\frac{\partial\Psi_i}{\partial\theta} = -K_i r\frac{\partial s_i}{\partial r} \tag{11}$$

By defining the dimensionless stream function as $\Psi_{Di} = \frac{\Psi_i}{2\pi K_i s_W}$, the Cauchy-Riemann equations read

$$\frac{\partial\Psi_{Di}}{\partial r_D} = \frac{1}{2\pi r_D}\frac{\partial s_{Di}}{\partial\theta} \tag{12}$$

$$\frac{\partial\Psi_{Di}}{\partial\theta} = -\frac{r_D}{2\pi}\frac{\partial s_{Di}}{\partial r_D} \tag{13}$$

Integration of (12)-(13) gives the following closed-form expression for the stream function in skin and formation zones

$$\Psi_{i,D} = -\frac{B_{i,0}\theta}{2\pi} - \left(A_{i,1} r_D - \frac{B_{i,1}}{r_D}\right)\frac{\sin\theta}{2\pi} \quad (14)$$

The term $-B_{i,0}\theta/2\pi$ represents the axisymmetric contribution of the well, while $-(A_{i,1}\, r_D - B_{i,1}/r_D)\, \sin\theta\, /\, 2\pi$ encodes the uniform ambient-flow deflection; together they delineate the stagnation points and the separatrix delimiting the capture zone. We set the integration constant so that $\Psi_{i,D} = 0$ on the separatrix, enabling direct plotting of capture-zone envelopes.

3.2. Special cases

As mentioned earlier, κ represents the heterogeneity ratio, controlling the resistance to flow in the skin zone. By adjusting κ to extreme values, different scenarios of flow behavior can be conceptualized. By letting $\kappa \to \infty$, the skin zone becomes fully impermeable and the formation zone drawdowns reduce to $s_{2,D} = \left(r_D + r_{s,D}^2/r_D\right)U_D \cos\theta$ in the limit when $R_D \to \infty$. This represents drawdown distribution around a circular impermeable obstacle of radius $r_{s,D}$ placed against a uniform flow. On the other hand, by letting $\kappa \to 0$, the skin zone behaves as a constant drawdown (head) boundary. Consequently, $s_{2,D} = 1 + \left(r_D - r_{s,D}^2/r_D\right)U_D \cos\theta$. This characterizes flow around a circular basin of radius $r_{s,D}$ which imposes a constant head condition. The solutions derived for these extreme cases are mathematically equivalent to those obtained by means of Joukowski conformal mapping techniques, as detailed by Bruggeman [24] (pp. 271 and 728). Essentially, these scenarios offer perspective on how the resistance in the skin zone influences the drawdown distribution and flow behavior near a well, ranging from impermeable barriers to constant head boundaries.

4. Results and discussion

4.1. General flow features

Detailed flow patterns around the well are presented for three cases: positive skin with $\kappa > 1$ (Fig. 2), no-skin ($\kappa = 1$) for reference (Fig. 3), and negative skin with $\kappa < 1$ (Fig. 4). Each case is subject to uniform ambient flow of varying strengths: U_D = 0.01, 0.03, and 0.05. In each case, the heterogeneity of the skin zone and aquifer formation caused a localized alteration of the uniform flow, leading to a diversion of the groundwater streamlines near these features. In the case of negative skin, the streamlines are directed toward the inner zone, which exhibited greater permeability compared to the surrounding medium (Fig. 4). Depending on their individual conductivity, streamlines either crossed through (Fig. 4) or flowed around the skin zone (Fig. 2). Similar patterns of streamlines can be identified in anisotropic aquifers with concentrically varying permeability due to blasting operations [25]. In each contour plot, the capture zone envelope is indicated by a thick dash-line. It comprises two branches that join together at the stagnation point, corresponding to two streamlines that bound the capture zone. In the direction of flow, the value of stream function remains zero on the left branch of the capture envelope while it is Q_D (Eq. (16)) on the right branch. Indeed, the difference between the functional values of $\Psi_{2,D}$ on the two branches exactly counterbalances the wellbore flow rate in each case, consistent with the water budget at the capture zone scale. In a similar context, Mahdavi [26] examined the preservation of mass balance during steady-state pumping in annular, wedge-shaped aquifers influenced by regional flow. The contrast in permeability (quantified by κ) between the formation and skin zones acts as a lens that either focuses or deflects groundwater streamlines. Analogous to Snell's law of optics, an incoming streamline that reaches the interzonal boundary at $r_D = r_{s,D}$ is refracted toward ($\kappa > 1$) or outward ($\kappa < 1$) from the boundary normal upon entering the skin

annulus. The flow outside the capture zone is bypassed by the well, and the condition of uniform flow is recovered at sufficiently large distances from the well. The strength of ambient flow further modulates these effects: at low U_D , the influence of heterogeneity dominates, while at higher U_D , the regional flow overwhelms local heterogeneities, compressing the capture zone and shifting the stagnation point upstream. Such complex interactions highlight the importance of accurately characterizing subsurface heterogeneity and ambient flow conditions when predicting well performance and designing remediation strategies.

Comparable flow patterns are observed during the continuous extraction of water from heterogeneous wedge-shaped aquifers, which are laterally bounded by either uniform streams [27] or boundary heads that vary along the stream-wise direction [11]. Additionally, akin to the phenomenon of well-bore clogging during hydraulic interference with ambient groundwater flow, the flow topology exhibits symmetry relative to the abscissa axis [28].

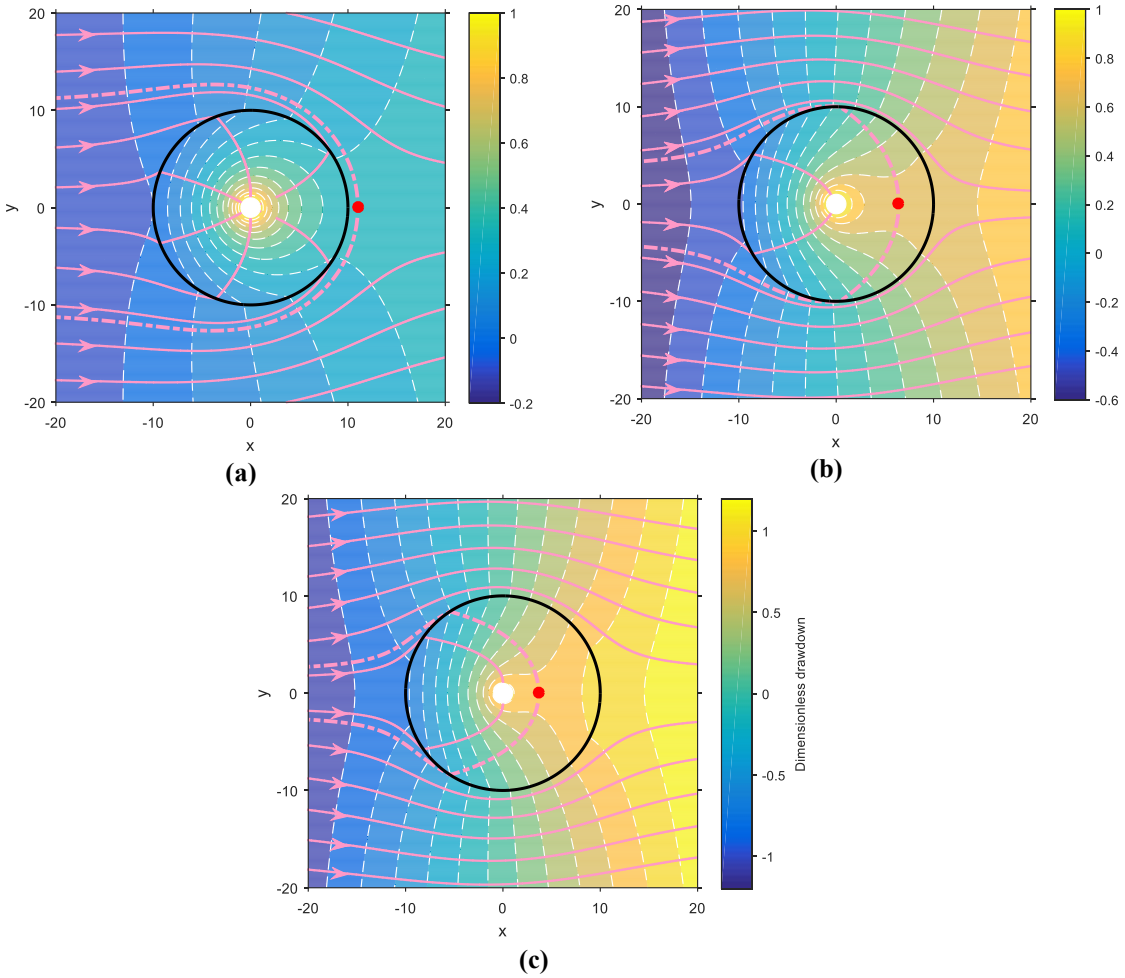


Fig. 2 Dimensionless drawdown contours with associated streamlines for different dimensionless ambient flow velocity U_D = (a) 0.01; (b) 0.03 and (c) 0.05 with κ fixed at 10. The pink dash-dotted line is the capture envelope, black solid line is the region of the skin zone, and the red circle is the location of stagnation point.

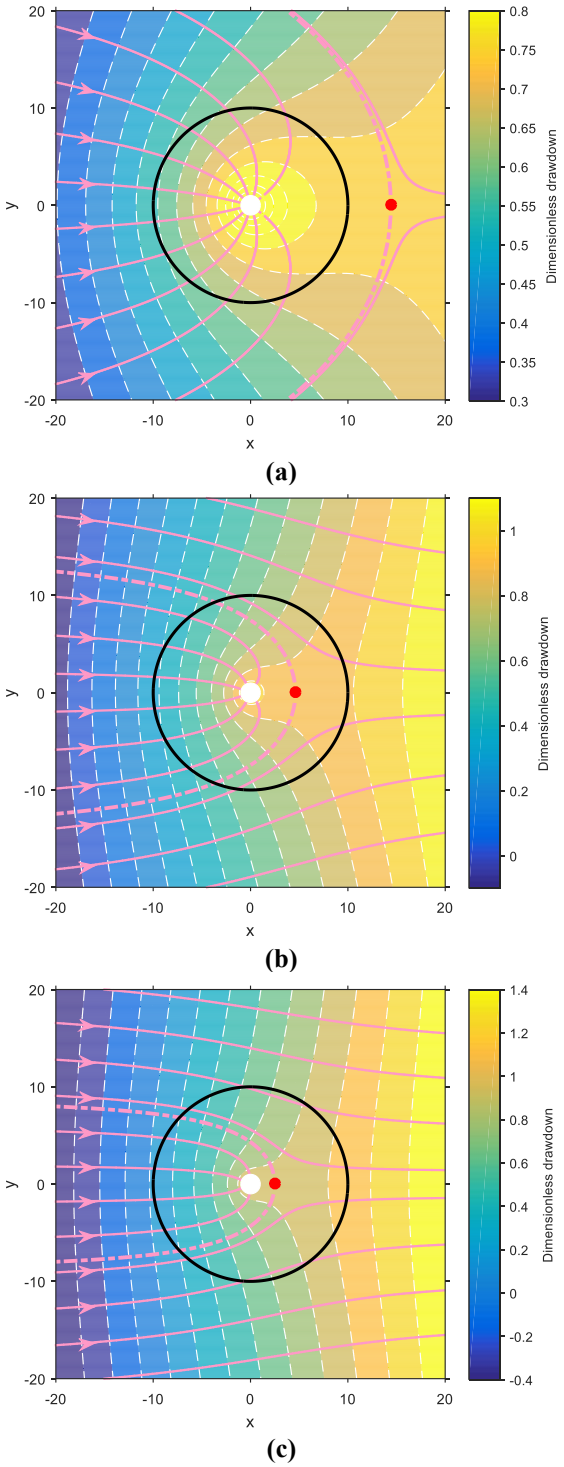


Fig. 3 Dimensionless drawdown contours with associated streamlines for different dimensionless ambient flow velocity $U_D =$ (a) 0.01; (b) 0.03 and (c) 0.05 with κ fixed at 1. The pink dash-dotted line is the capture envelope, black solid line is the region of the skin zone, and the red circle is the location of stagnation point.

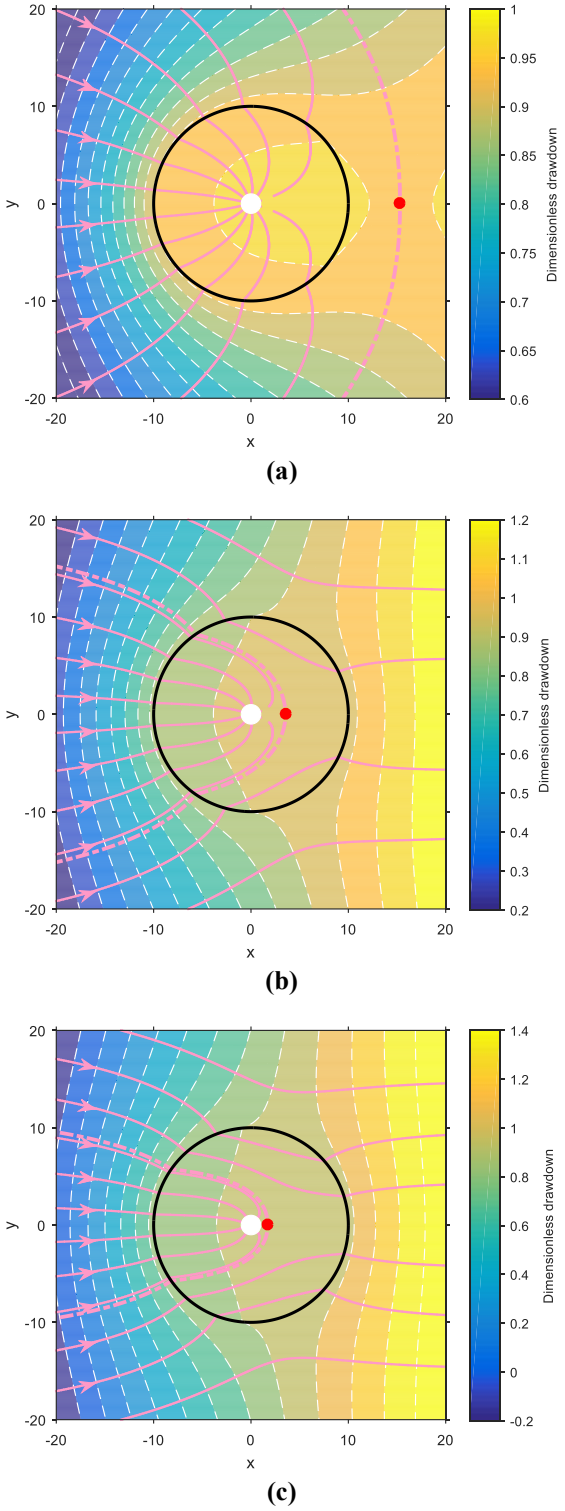
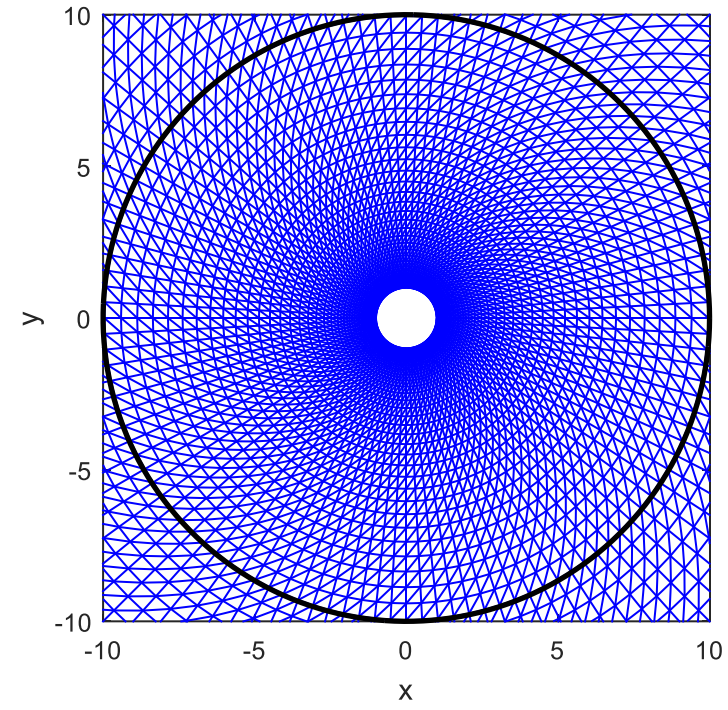


Fig. 4 Dimensionless drawdown contours with associated streamlines for different dimensionless ambient flow velocity U_D = (a) 0.01; (b) 0.03 and (c) 0.05 with κ fixed at 0.1. The pink dash-dotted line is the capture envelope, black solid line is the region of the skin zone, and the red circle is the location of stagnation point.

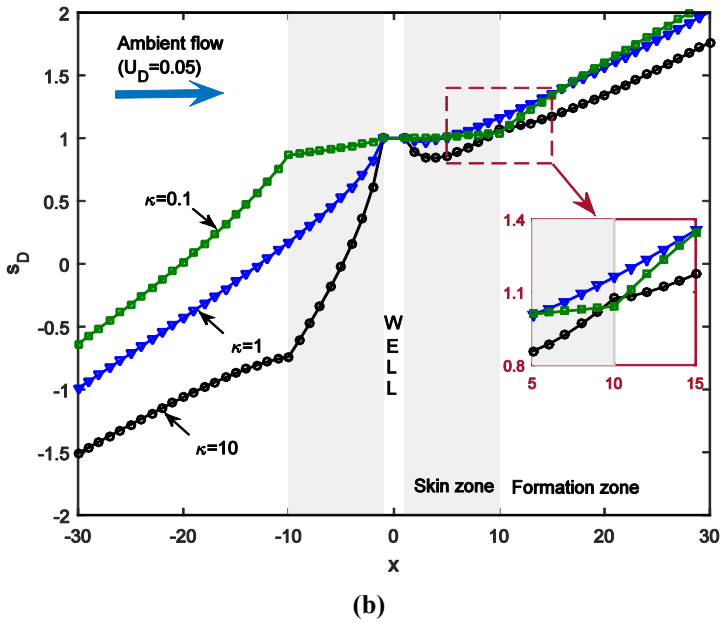
4.2. Comparing to finite element solution

To confirm the validity of the drawdown distribution described in Eq. (9), it is possible to verify it through direct substitution and ensure that it adheres to the model Eq. (1) and associated boundary conditions in Eqs. (2)–(7). Alternatively, the results are validated by comparing them with those obtained from the Matlab Finite Element Toolbox "pdetool". This toolbox allows addressing a range of 2-D groundwater hydraulics problems involving the elliptic model of the form $\frac{\partial}{\partial x}\left(\tau\frac{\partial s}{\partial x}\right)+\frac{\partial}{\partial y}\left(\tau\frac{\partial s}{\partial y}\right)=0$ under any desired combination of Dirichlet and Neumann boundary conditions [26]. The Cartesian coordinate system (x,y) has its origin at the well axis, thereby obeying the relations $x=r_D\cos\theta$ and $y=r_D\sin\theta$ (dimensionless). The computational domain representing the flow system consists of a circular region with a concentric hollow representing the well. The outer circle has a radius R_D, while the inner hollow has a radius 1. On the exterior and interior circumfences of the domain the Dirichlet boundary condition $s_D=U_Dx$ (corresponding to Eq. (7)) and $s_D=1$ are imposed, respectively. The radial variation in hydraulic conductivity is accounted for by setting $\tau=K_2/\kappa$ if $1\le x^2+y^2\le r_{s,D}^2$ (skin zone) and $\tau=K_2$ if $r_{s,D}^2<x^2+y^2\le R_D^2$ (formation zone). In other words, the value of K_2 remained the same in all computations but K_1 was set in accordance with the specific value of κ chosen in each case. At the start of computation, the domain is discretized with a relatively coarse mesh of triangular elements (Fig. 5a). As the computation progresses, finite elements are adaptively refined, resulting in smaller triangles near the well. This refinement is particularly important in areas where drawdowns vary significantly over distance [27]. The iterative process stops when the changes in the solution between two successive refinements fall below a predefined tolerance.

Figure 5b displays the spatial distribution of the drawdown predicted by the proposed solution and the finite element solution with $\kappa=0.1$, 1, and 10 and $U_D=0.05$. The results are computed along the flow axis of symmetry, $y_D=0$ for $r_{s,D}=10$ and $R_D=1000$. By decreasing the value of κ, the skin zone becomes less resistant to flow and more water is conveyed laterally toward the well. This in turn facilitates hydraulic adjustment of skin zone drawdowns to the piezometric level at the wellbore. The curve for $\kappa=0.1$ demonstrates this by becoming almost uniform around $s_D=1$ in the skin zone. As κ approaches zero, the skin zone exhibits minimal flow resistance, behaving like a constant drawdown boundary. In this case, the drawdown reaches $s_D=1$ throughout the skin zone, as described by Eq. (9). The curves maintain continuity of drawdown across the skin-formation interface, and their radial slopes reflect the heterogeneity of the aquifer. The zoomed-in view in Fig. 5b confirms these subtle variations, which are influenced by the aquifer's heterogeneity. Comparable patterns were identified at the inter-zonal boundary of a heterogeneous aquifer consisting of two zones with internally homogeneous materials, each featuring a set of randomly positioned pumping/injection wells [27]. Notably, the drawdown curves predicted by the proposed and finite element solutions exhibit very close agreement in Fig. 5b.



(a)



(b)

Fig. 5 (a) Zoomed view of the triangular mesh layout (b) Spatial distribution of dimensionless drawdown computed by the proposed solution (solid lines) and finite element solution (symbols).

To assess the precision of the analytical solution, a more quantitative analysis was conducted between the computed drawdowns and those obtained from the finite element method across three representative heterogeneity ratios, as illustrated in Fig. 5b. For each selected value of the heterogeneity parameter κ (0.1, 1, and 10), the Root Mean Square Error (RMSE) was calculated to quantify the discrepancy between the analytical and numerical solutions. The resulting RMSE values were 1.95×10^{-4} for $\kappa = 0.1$, 7.36×10^{-7} for $\kappa = 1$ and 1.12×10^{-5} for $\kappa = 10$. These consistently low RMSE values across all tested κ indicate a high degree of agreement between the two approaches. Notably, the smallest error occurs at κ = 1, suggesting optimal alignment in homogenous case. Overall, the results validate the robustness of the finite element formulation in accurately replicating the analytical drawdown behavior under varying degrees of subsurface heterogeneity.

We acknowledge that no field-site application or pumping-test dataset is analyzed here; the study focuses on analytical development and numerical validation. The absence of a real-aquifer test limits immediate applied generalization, and future work will incorporate pumping-test data to benchmark against established constant-rate solutions (e.g., Theis) and standard capture-zone models.

4.3. Locus of stagnation points

Determination of stagnation point is a crucial step in delineation of well capture zone. The physical significance of the stagnation point lies in its role as a boundary marker for the well's capture zone, where groundwater flow transitions from being influenced by regional ambient conditions to being dominated by the pumping-induced drawdown. Stagnation point can be recognized as a location in the flow field where both the radial and angular components of the Darcian velocity vanish [29]. This approach facilitates the identification of flow stagnation points within a three-component composite structure, consisting of a vertical or horizontal well, a gravel pack, and an annular skin, under continuous pumping conditions [28].

For positive values of wellbore drawdown (i.e., $s_w > 0$ due to pumping), stagnation point must lay downstream from the well along ray $\theta = 0$ which represents the axis of symmetry of the flow field. The radial position of stagnation point is governed by the quadratic equation $A_{i,1}r_D^2 + B_{i,0}r_D - B_{i,1} = 0$ resulting from $\partial s_{i,D}/\partial r_D = 0$ which identifies a location where there is no change in hydraulic drawdown gradient with respect to radial coordinate.

Letting $\Delta_i = B_{i,0}^2 + 4A_{i,1}B_{i,1}$ and expressing the real positive root (since only physical, real distances are expected) as $r_{stag,D} = \left(\sqrt{\Delta_i} - B_{i,0}\right)/2A_{i,1}$, two scenarios can be considered separately: For $i = 1$, if $r_{stag,D}$ falls between 1 (wellbore radius) and $r_{s,D}$ (outer radius of the skin zone), then stagnation point is at $\left(r_{stag,D}, 0\right)$ in the skin annulus. Similarly, flow stagnates in the formation zone if there exists a root between $r_{s,D}$ (skin zone boundary) and R_D (formation zone radius) for $i = 2$. Summarizing, this implies that the exact position of stagnation point depends on the flow regime and the geometry of the zones surrounding the well, with its location derived from solving the quadratic equation under specific conditions.

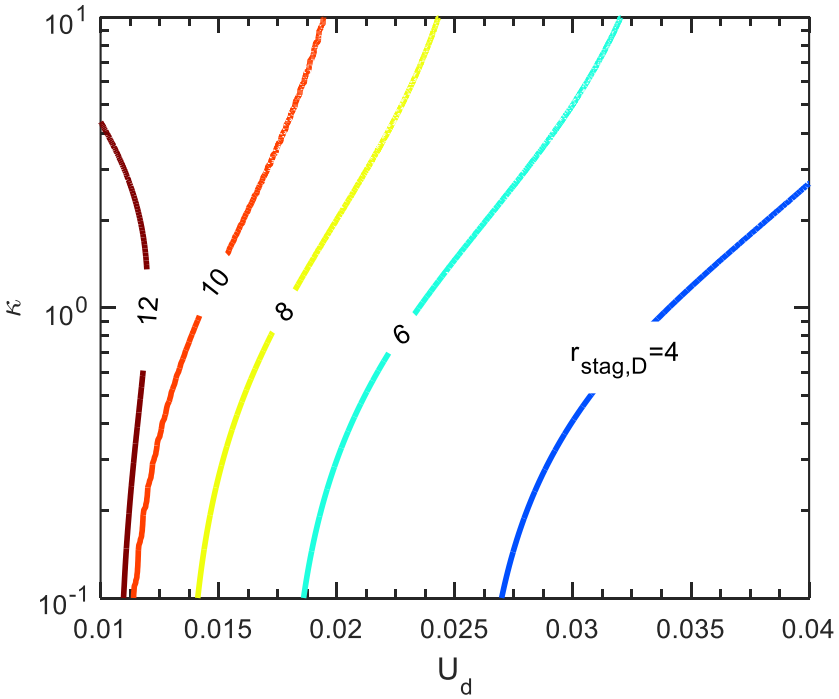


Fig. 6 Locus of the stagnation point in the flow field, illustrating the influence of changes in the ambient flow velocity U_D and the hydraulic conductivity ratio κ.

Fig. 6 shows how locus of stagnation point is affected in response to changes in U_D and κ, keeping the other parameters same as before. The contour lines are labeled according to the radial position of stagnation point, $r_{stag,D}$, discussed above. It is seen that the location of this point is highly sensitive to both the heterogeneity of the subsurface and the strength of the ambient flow. A number of observation can be made from the contour plot: (i) Of special interest is the contour line $r_{stag,D} = r_{s,D}$ which divides the solution space to two sub-regions: for those pairs of (U_D, κ) that fall on the right side of this contour line, stagnation points falls in the skin zone ($r_{stag,D} < r_{s,D}$), while the region on the left of this contour line corresponds to the stagnation points arising in the formation zone ($r_{stag,D} > r_{s,D}$); (ii) For a certain value of κ, stagnation point tends to shift in the upstream direction as the value of U_D increases. Accordingly, the strength of ambient flow is large enough to locally vanish flow velocities in the close vicinity of the well, forcing the stagnation point to form at a shorter distance from the well; (iii) For a certain value of U_D, there exists two distinct values of κ possessing the same $r_{stag,D}$ in the formation zone. This indicates that different levels of heterogeneity can lead to identical stagnation point positions under specific flow conditions, implying the non-uniqueness of capture zone geometry in heterogeneous aquifers.

4.4. Wellbore flow rate

In accordance with the Darcy's law for radial flow, the wellbore flow rate per unit aquifer thickness is given by $Q = \int_0^{2\pi} u_1(r_W, \theta)\, r_W \mathrm{d}\theta$. In the dimensionless form it can be expressed as

$$Q_D = \frac{1}{2\pi K_2 s_W} \int_0^{2\pi} -K_1 \left.\frac{\partial s_1}{\partial r}\right|_{r=r_W} r_W \,\mathrm{d}\theta = -\frac{1}{\kappa} \int_0^{2\pi} \left.\frac{\partial s_{1,D}}{\partial r_D}\right|_{r_D=1} \mathrm{d}\theta \tag{15}$$

which results in

$$Q_D = \frac{1}{\ln\left(r_{s,D}^{\kappa-1} R_D\right)} \quad (16)$$

For the case of homogeneous aquifer ($\kappa = 1$), Eq. (16) reduces to $Q_D = 1/\ln R_D$. This result can be expressed in terms of physical variables as $s_W = \frac{Q}{2\pi K_2} \ln\left(\frac{R}{r_W}\right)$ which corresponds to the Thiem formula for calculating drawdown due to a well pumping at a constant rate [29]. Fig. 7 depicts variation of wellbore flow rate, Eq. (16), in response to changes in $r_{s,D}$ and κ, with each contour line labeled by the associated Q_D. A reduction in heterogeneity ratio reflects a higher value of K_1 if the hydraulic conductivity of formation zone, K_2, is kept constant. In a two-zone aquifer model, the near-well region and the surrounding formation exhibit distinct hydraulic conductivities, collectively governing the ease with which water flows into the well [30,31].

When $\kappa > 1$, the outer formation exhibits higher permeability than the skin zone, which imposes a flow restriction. In this scenario, water must traverse the lower-permeability skin zone to reach the well, effectively creating a bottleneck. An increase in the radius of the skin zone corresponds to a larger fraction of the flow path being occupied by this low-permeability region, resulting in heightened effective resistance. According to Darcy's law for radial flow, this leads to a reduction in the dimensionless wellbore flow rate Q_D, as illustrated in Fig. 7 for $\kappa > 1$.

Conversely, when $\kappa < 1$, the skin zone exhibits greater permeability than the surrounding formation, thereby facilitating a preferential pathway for water to enter the well. Expanding the radius of this high-permeability zone increases the region through which water can move efficiently towards the well, enhancing the effective conductivity within the near-well region. This results in an overall increase in the wellbore flow rate, as illustrated in Fig. 7 for $\kappa < 1$.

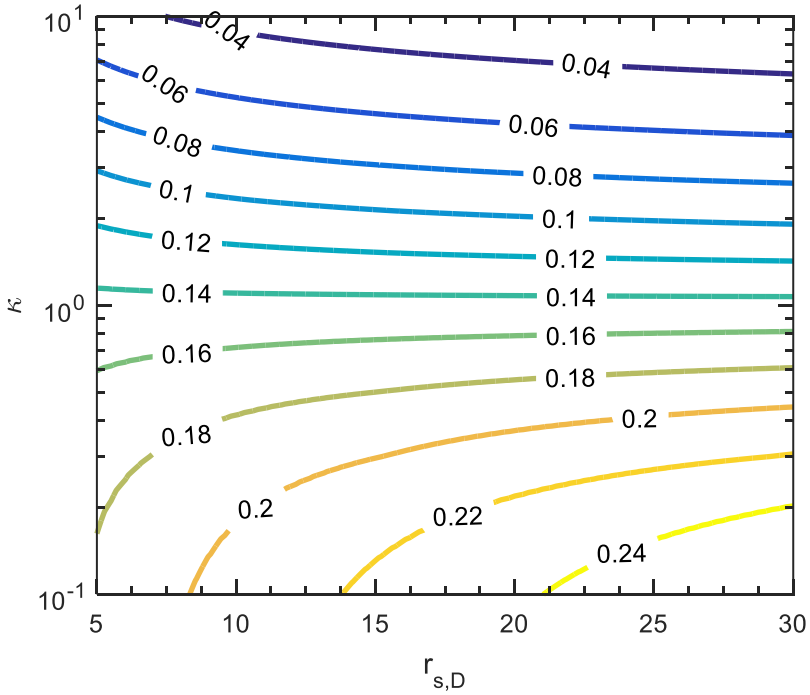


Fig. 7 Variation in wellbore flow rate showing the influence of changes in the dimensionless radius of skin zone $r_{s,D}$ and the hydraulic conductivity ratio κ.

4.5. Groundwater transit time

Groundwater transit time refers to the time it takes for water to move from its recharge point in the groundwater system to its discharge point, such as a stream or lake. In other words, it determines the duration between water entering and leaving the aquifer. This concept is essential for understanding the fate of chemical constituents in groundwater. For instance, pollutants may undergo degradation reactions during their residence time in the aquifer, impacting their concentration and distribution. While analytical solutions exist for groundwater transit time in more idealized or homogeneous systems [32], the complexity introduced by heterogeneity under pumping conditions remains a significant challenge. Indeed, variations in permeability and localized hydraulic responses make it difficult to develop a one-size-fits-all analytical model [22-23]. Motivated by this research gap, the next paragraphs attempt to analytically track the movement of individual fluid particles along a defined path, monitoring their positions over time while accounting for heterogeneity within a Lagrangian framework. Physically, heterogeneity alters the hydraulic conductivity landscape, creating zones of preferential flow or resistance that fluid particles must navigate.

For our purpose, the transit time, defined as the time it takes for a fluid particle to travel from the radius of influence to the wellbore along the flow axis of symmetry (shortest path), can be expressed as $T = \int_R^{r_s} \mathrm{d}r/u_2(r,\pi) + \int_{r_s}^{r_w} \mathrm{d}r/u_1(r,\pi)$ where $u_i = (K_i/n_e)\partial s_i/\partial r$ is the radial component of the groundwater velocity and n_e is effective porosity. Converting to dimensionless form $T_D = K_2 s_w T/r_w^2 n_e$ yields

$$T_D = \int_{R_D}^{r_{s,D}} \frac{\mathrm{d}r_D}{\left.\frac{\partial s_{D2}}{\partial r_D}\right|_{\theta=\pi}} + \int_{r_{s,D}}^{1} \frac{\kappa \mathrm{d}r_D}{\left.\frac{\partial s_{D1}}{\partial r_D}\right|_{\theta=\pi}} \tag{17}$$

Evaluating the integrals offers a closed-form expression for the dimensionless transit time

$$T_D = F_2(r_{s,D}) - F_2(R_D) + \kappa F_1(1) - \kappa F_1(r_{s,D}) \tag{18}$$

with the lumped function $F_i(\omega)$ defined as

$$F_i(\omega) = -\frac{\omega}{A_{i,1}} - \frac{B_{i,0}}{2A_{i,1}^2}\ln(A_{i,1}\omega^2 - B_{i,0}\omega - B_{i,1}) + \left(\frac{B_{i,0}^2}{A_{i,1}^2} + 2\frac{B_{i,1}}{A_{i,1}}\right) \times \begin{cases} \frac{1}{\sqrt{\Delta_i}}\tanh^{-1}\left(\frac{2A_{i,1}\omega - B_{i,0}}{\sqrt{\Delta_i}}\right) & \text{if } \Delta_i > 0 \\ \frac{-1}{\sqrt{-\Delta_i}}\tan^{-1}\left(\frac{2A_{i,1}\omega - B_{i,0}}{\sqrt{-\Delta_i}}\right) & \text{if } \Delta_i < 0 \end{cases} \tag{19}$$

As Fig. 8 illustrates, when the strength of ambient flow increases, transit times are reduced, indicating that fluid particles move faster under stronger ambient flow conditions. This observation aligns with findings from recent studies, such as [33], which highlight the variability in transit times and tortuosity in fractured rock models with small-scale heterogeneity.

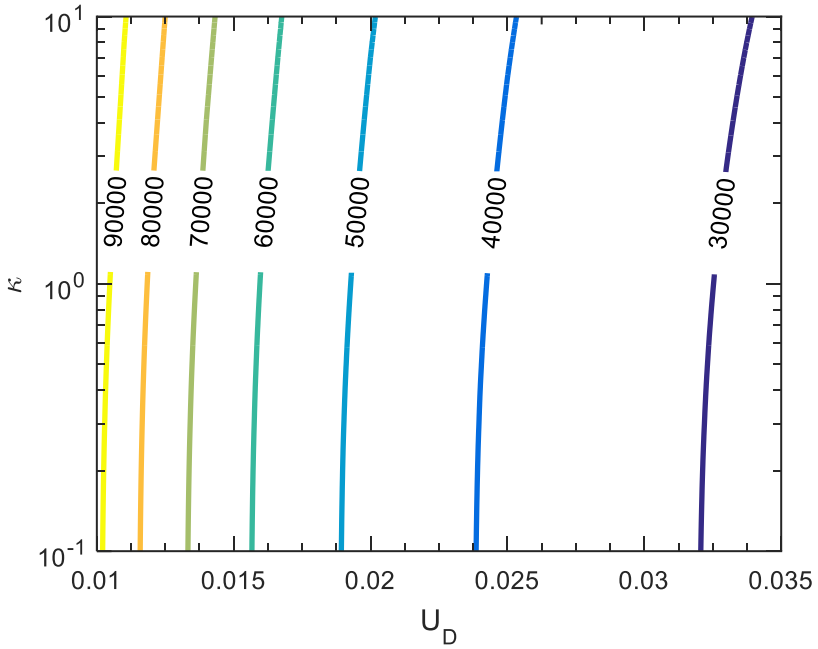


Fig. 8 Variation in groundwater transit time illustrating the influence of changes in the ambient flow velocity U_D and the hydraulic conductivity ratio κ.

Furthermore, an increase in heterogeneity ratio corresponds to a lower value of K_1, while keeping K_2 unchanged. Higher κ implies greater resistance to flow in the skin zone, leading to increased transit times. This again highlights the role of heterogeneity in influencing flow dynamics, transit time distributions, predicting contaminant travel times, assessing aquifer vulnerability, and designing effective remediation strategies in heterogeneous environments.

4.6 Parameter estimation

This section examines how the present solution allows us to estimate the hydraulic conductivity of the skin zone and ambient flow velocity, given the observed (measured) drawdowns in the formation zone. All draws on data use dimensionless drawdown s_D at prescribed r_D and θ. This inverse problem is formulated as the minimization of an objective function, which typically aims to minimize the least squared differences between calculated and observed drawdowns (residuals). For this purpose, the objective function can be defined as follows:

$$\text{Objective function} = \frac{1}{2}\sum_{j=1}^{M}\left(s^{(j)} - {s_{Obs}}^{(j)}\right)^2 \tag{20}$$

where $s^{(j)}$ and ${s_{Obs}}^{(j)}$ are j-th modeled drawdown and observed drawdown data and M is the total number of observation. In the parameter-estimation procedure, K_1 and U are treated as the two unknown model parameters which are simultaneously determined by minimizing the objective function, Eq. (20), using the available monitoring-well observations. Thus, the estimation procedure seeks to recover the parameter pair (K_1, U) from the prescribed observations. The modeled drawdowns are based on Eq. (9) for any value of K_1 and U encountered in the minimization process. Following the method proposed in [34], the observed drawdowns can be taken as synthetic data. These are generated by imposing a random noise on the drawdowns

computed from the proposed solution, with the noise amplitudes not exceeding $\varepsilon = \pm 10\%$ of the base drawdowns at every observed data. The random noise has a zero-mean Gaussian distribution. The observed drawdowns are calculated by setting $K_1 = 2$ m/d, $K_2 = 10$ m/d, $R = 1000$ m, $r_w = 0.1$ m, $r_s = 1$ m, $s_w = 10$ m, and $U = 10^{-3}$ m/d. To monitor the flow patterns and gradients in the aquifer, a total number of $M = 19$ equidistant observation points are located upstream of the well along the direction of ambient flow ($r_j = j \times 50\text{m}$ for $j = 1$ to 19). The objective function is minimized by simultaneously setting its derivatives with respect to κ and U_D equal to zero:

$$\begin{cases} \sum_{j=1}^{M} \left(s^{(j)} - {s_{Obs}}^{(j)}\right) \dfrac{\partial s^{(j)}}{\partial \kappa} = 0 \\ \sum_{j=1}^{M} \left(s^{(j)} - {s_{Obs}}^{(j)}\right) \dfrac{\partial s^{(j)}}{\partial U_D} = 0 \end{cases} \quad (21)$$

This system of two non-linear algebraic equations is then submitted to the Maple® built-in function "fsolve". This gives $K_{1,Est.} = 2.05$ m/day and $U_{Est.} = 1.05 \times 10^{-3}$ m/d for which objective function attains a minimum of 1.46×10^{-4}. The estimated (optimal) values fall within, respectively, 2.5% and 5% margins of the target values $K_1 = 2$ m/d and $U = 10^{-3}$ m/d. A similar computation with a higher noise level of $\varepsilon = \pm 20\%$ yields parameter estimates of $K_{1,Est.} = 1.99$ m/day and $U_{Est.} = 1.05 \times 10^{-3}$ m/d with the objective function attaining a minimum value of 2.65×10^{-4}.

Figure 9 compares the observed and calculated drawdowns and shows favorable agreement across the observation points for both $\varepsilon = \pm 10\%$ and $\varepsilon = \pm 20\%$. For perfectly observed data ($\varepsilon = 0$), the algorithm recovers the base values of K_1 and U exactly, driving the objective function to 5×10^{-20}.

To examine the robustness of parameter estimation with respect to the monitoring-well configuration, an alternative layout comprising 19 monitoring wells was considered. The wells were distributed over the radial domain $r_D < R_D$, with radial distances selected to provide adequate coverage of both the near-well and far-field regions. The angular coordinates were varied to avoid an overly regular spatial arrangement and to provide a more irregular distribution around the pumping well. The radial and angular coordinates of the monitoring wells are listed in Table 2, while their corresponding spatial layout is shown in Fig. 10. the estimated parameters are $K_{1,Est.} = 2.05$ m/day and $U_{Est.} = 1.01 \times 10^{-3}$ with the objective function attaining a minimum value of 8.2×10^{-4}. This alternative configuration provides an independent assessment of the estimated parameters and reduces the potential influence of the original monitoring-well arrangement.

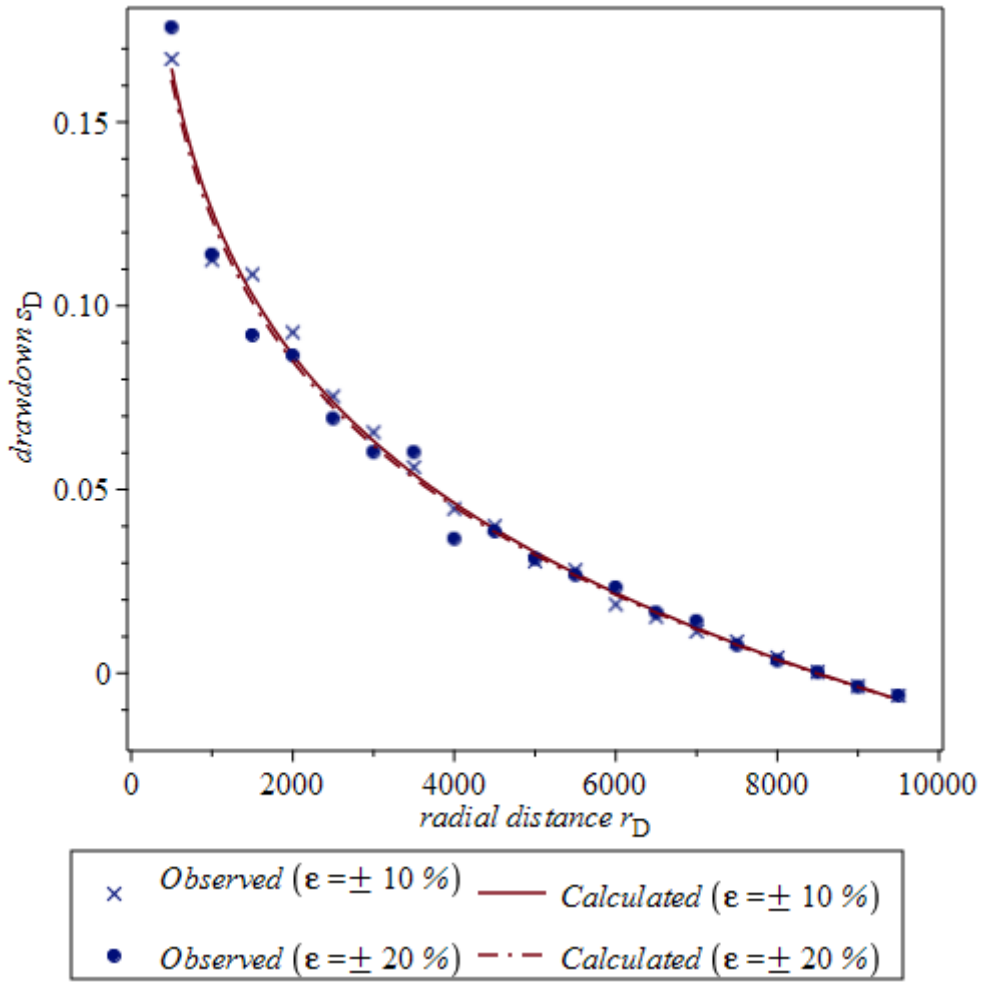


Fig. 9 Spatial distribution of dimensionless drawdown computed by the proposed solution and the observed drawdown data.

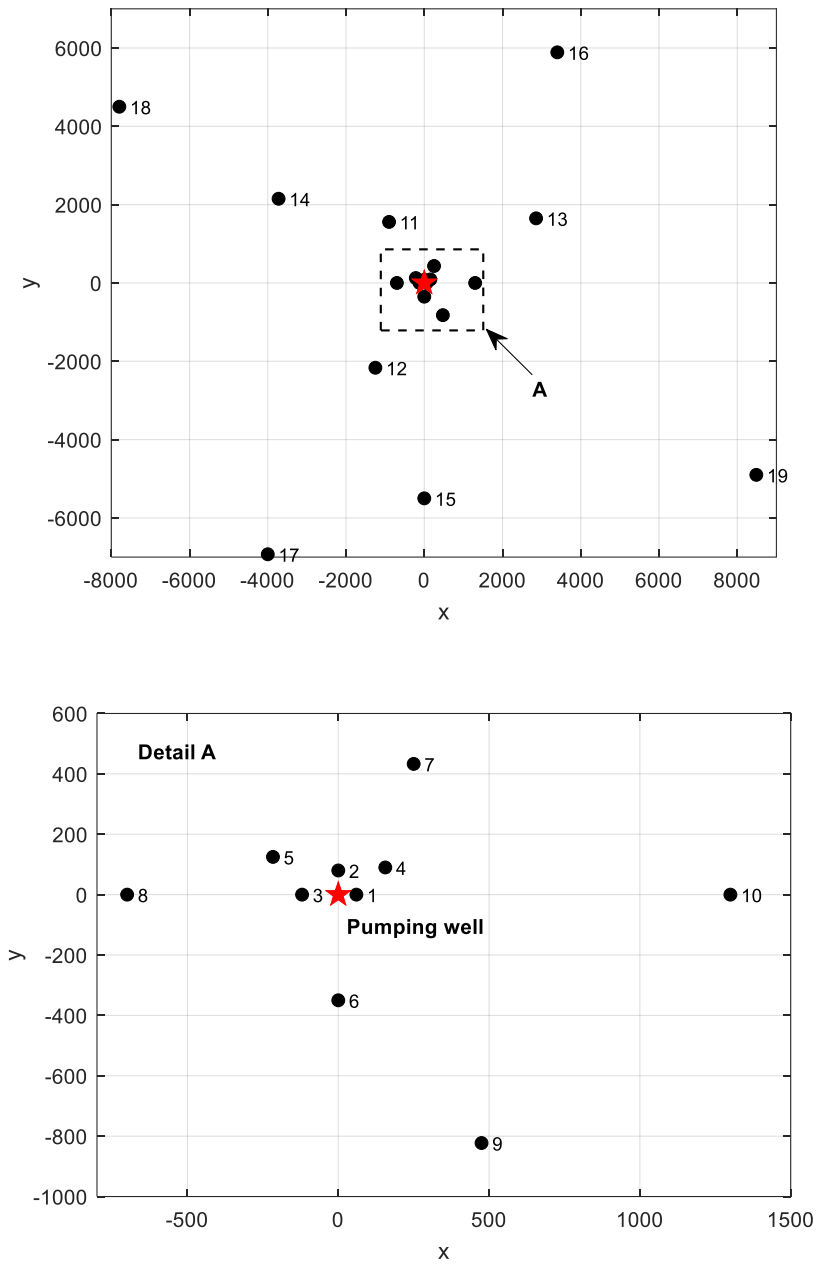


Fig. 10 Alternative irregular monitoring-well layout for parameter estimation.

5. Summary and conclusions

The present study investigates groundwater flow behavior around constant-head pumping wells in two-zone heterogeneous aquifers under unidirectional ambient flow received from remote ends of the flow system. Extremely simple analytical expressions were derived for steady-state drawdown distribution in both the skin and formation zones. The closed-form solutions were then integrated according to the Cauchy-Riemann equations to obtain flow stream function. This allows analytical description of the flow net around the well, satisfying the refraction of streamlines across the interface between the skin and formation zones. Key aspects of model response to changes in ambient flow velocity and heterogeneity ratio of the aquifer were examined and a number of conclusions can be drawn:

(i) Analytical expressions have been derived for two branches of capture-zone envelope. Along these streamlines, the stream function evaluates to zero on one branch, while on the other branch, it corresponds to the well discharge. This is consistent with the steady-state mass balance at the capture zone scale, where the amount of water that enters the capture zone must be offset by the amount that is abstracted by the well.

(ii) Negative skins which are characterized by a heterogeneity ratio less than one ($\kappa < 1$), establishes a moderately uniform drawdown across the skin zone. Deviations from this occur by increasing κ in the case of positive skins (Fig. 5b).

(iii) Capture width narrows as ambient flow U_D increases, and likewise narrows with increasing heterogeneity ratio κ. Accordingly, stronger ambient flow or higher κ reduces the area from which the well draws water.

(iv) A critical contour line in (U_D, κ) space is delineated which assists in determining whether the stagnation point lies within the skin zone or the formation zone (Fig. 6).

(v) As the strength of ambient flow increases, the stagnation point moves upstream, closer to the well. Stronger ambient flow locally reduces flow velocities downstream of the well, leading to a shorter distance to the stagnation point. Stagnation points tend to move downstream in response to an increase in the heterogeneity ratio (Fig. 6).

(vi) The skin zone's effect on wellbore flow rate is twofold: when the hydraulic conductivity of the skin zone is lower than that of the surrounding formation ($\kappa > 1$), it acts as a barrier to flow. An increase in the skin radius signifies a larger low-permeability region, leading to greater resistance to flow. Consequently, the wellbore flow rate (Q_D) decreases. Conversely, when the hydraulic conductivity of the skin zone exceeds that of the surrounding formation ($\kappa < 1$), the skin zone functions as a conduit that facilitates flow. Expanding the radius of this high-permeability region reduces flow resistance near the well, effectively enhancing the wellbore flow rate (Fig. 7).

(vii) By defining the transit time as the duration over which a fluid particle travels from the radius of influence to the wellbore along its shortest path, it is examined how stronger ambient flow reduces transit time, while increased resistance due to higher heterogeneity ratio of positive skins prolong it (Fig. 8).

Furthermore, an analytical framework was developed to estimate key parameters of the model characterizing ambient flow and heterogeneity of the aquifer based on the observed drawdowns (Fig. 9). This

hydrogeological characterization aims to improve our understanding of groundwater flow, hydraulic parameters, geological materials, and flow rates. It should be noted that the present study is analytical in nature, and the finite-element comparison provides numerical verification of the derived solution rather than independent physical validation. Field observations or pumping-test data were not considered in this study. Consequently, the predictive capacity must still be demonstrated against observed constant-head pumping responses before operational adoption. Future work will (i) apply the framework to published and operational constant-head tests, (ii) provide side-by-side benchmarks against constant-rate analytical and numerical models, and (iii) assess sensitivity to observation-network design and measurement noise. Field datasets of time-varying drawdown, discharge, and water-quality metrics from managed pumping tests will be acquired to calibrate and stress-test the solution. These deployments will assess the feasibility of maintaining constant heads, quantify measurement uncertainty, and refine the parameter-estimation workflow for sparse monitoring networks.

Funding Statement: This is not applicable

Conflict of Interest: The authors declare that they have no conflict of interest.

AI Statement: The author(s) did not use AI tools for conducting this research.

Author Contributions: All authors contributed to the study conception, design, material preparation, analysis, writing first draft and final version of the manuscript.

List of symbols

K_1: Hydraulic conductivity of skin zone [LT^{-1}]
K_2 : Hydraulic conductivity of formation zone [LT^{-1}]
Q: Wellbore flow rate per unit aquifer thickness [L^2T^{-1}]
r: Distance from the well axis [L]
R: Outer radius of formation zone [L]
r_s: Outer radius of skin zone [L]
r_W: Wellbore radius [L]
s_1: Drawdown in skin zone [L]
s_2: Drawdown in formation zone [L]
s_W: Drawdown at wellbore [L]
T: Groundwater transit time [T]
U: Ambient flow velocity [LT^{-1}]
$Q_D = Q/(2\pi K_2 s_W)$: Dimensionless wellbore flow rate [-]
$r_D = r/r_w$: Dimensionless distance from well axis [-]
$R_D = R/r_w$: Dimensionless radius of formation zone [-]
$r_{s,D} = r_s/r_w$: Dimensionless radius of skin zone [-]
$r_{stag,D} = r_{stag}/r_w$: Dimensionless position of stagnation point [-]
$s_{Di} = s_i/s_w$: Dimensionless drawdown [-]
$U_D = Ur_w/(K_2 s_w)$: Dimensionless velocity of ambient flow [-]
$\kappa = K_2/K_1$: Hydraulic conductivity ratio [-]
Ψ_1: Stream function in skin zone [L^2T^{-1}]
Ψ_2: Stream function in formation zone [L^2T^{-1}]
$\Psi_{Di} = \Psi_i/(2\pi K_i s_W)$ Dimensionless stream function [-]
Subscript "D": Dimensionless variable
Subscript "*i*": Variable belonging to skin zone (*i*=1) or formation zone (*i*=2)

References

1. Foster S, Chilton J, Nijsten GJ, Richts A. Groundwater—a global focus on the 'local resource'. Current opinion in environmental sustainability. 2013; 5(6):685-95. https://doi.org/10.1016/j.cosust.2013.10.010
2. Flindt Jørgensen L, Villholth KG, Refsgaard JC. Groundwater management and protection in Denmark: a review of pre-conditions, advances and challenges. International journal of water resources development. 2017; 33(6):868-89. https://doi.org/10.1080/07900627.2016.1225569
3. Li P, Karunanidhi D, Subramani T, Srinivasamoorthy K. Sources and consequences of groundwater contamination. Archives of environmental contamination and toxicology. 2021;80(1):1-0. https://doi.org/10.1007/s00244-020-00805-z
4. Narimani R, Murgulet I, Murgulet D. Emerging Contaminants in Groundwater: Challenges, Management, and Policy Perspectives. In Emerging Pollutants: Protecting Water Quality for the Health of People and the Environment (pp. 189-226). 2025; Cham: Springer Nature, Switzerland.
5. Bau DA, Mayer AS. Stochastic management of pump-and-treat strategies using surrogate functions. Advances in water resources. 2006; 29(12):1901-1917. https://doi.org/10.1016/j.advwatres.2006.01.008
6. Carroll KC, Brusseau ML, Tick GR, Soltanian MR. Rethinking pump-and-treat remediation as maximizing contaminated groundwater. Science of the Total Environment. 2024; 918:170600. https://doi.org/10.1016/j.scitotenv.2024.170600
7. Matott LS, Rabideau AJ, Craig JR. Pump-and-treat optimization using analytic element method flow models. Advances in Water Resources. 2006; 29(5):760-75. https://doi.org/10.1016/j.advwatres.2005.07.009
8. Faisal AA, Sulaymon AH, Khaliefa QM. A review of permeable reactive barrier as passive sustainable technology for groundwater remediation. International Journal of Environmental Science and Technology. 2018;15(5):1123-38. https://doi.org/10.1007/s13762-017-1466-0
9. Frind EO, Muhammad DS, Molson JW. Delineation of three-dimensional well capture zones for complex multi-aquifer systems. Groundwater. 2002; 40(6):586-98. https://doi.org/10.1111/j.1745-6584.2002.tb02545.x
10. Anderson MP, Woessner WW, Hunt RJ. Applied ground water modeling: simulation of flow and advective transport. Academic press. 2015.
11. Mahdavi A. Well hydraulics in dual-zone heterogeneous wedge-shaped aquifers under an ambient flow from stream-wise varying boundary heads. Journal of Hydrology. 2022; 612:128063. https://doi.org/10.1016/j.jhydrol.2022.128063
12. Nagheli S, Samani N, Barry DA. Capture zone models of a multi-well system in aquifers bounded with regular and irregular inflow boundaries. Journal of Hydrology X. 2020; 7, 100053. https://doi.org/10.1016/j.hydroa.2020.100053
13. Zhang S, Wang XS. Regional Flow Influenced Recirculation Zones of Pump–and–Treat Systems for Groundwater Remediation with One or Two Injection Wells: An Analytical Comparison. Water. 2023;15(15):2852. https://doi.org/10.3390/w15152852
14. Ciftci E. A practical approach for the interpretation of flowing well tests. Arabian Journal of Geosciences. 2018; 11(23):761. https://doi.org/10.1007/s12517-018-4137-7
15. Hiller CK, Levy BS. Estimation of aquifer diffusivity from analysis of constant-head pumping test data. Groundwater. 1994; 32(1):47-52. https://doi.org/10.1111/j.1745-6584.1994.tb00610.x
16. Chen CS, Chang CC. Use of cumulative volume of constant-head injection test to estimate aquifer parameters with skin effects: Field experiment and data analysis. Water Resources Research. 2002; 38(5):14-1. https://doi.org/10.1029/2001WR000300
17. Perina T. General well function for soil vapor extraction. Advances in Water Resources. 2014; 66:1-7.

https://doi.org/10.1016/j.advwatres.2014.01.005
18. Lin YC, Yeh HD. New analytical model for constant-head pumping: Considering rate-dependent factor at well screen. Journal of Hydrology. 2020; 581:124395. https://doi.org/10.1016/j.jhydrol.2019.124395
19. Bashandy AM, Bekhit HM, Radwan HG. Uncertainty assessment of aquifer hydraulic parameters from pumping test data. Applied Water Science. 2024; 14(4):84. https://doi.org/10.1007/s13201-024-02134-1
20. Dashti Z, Nakhaei M, Vadiati M, Karami GH, Kisi O. A literature review on pumping test analysis (2000–2022). Environmental Science and Pollution Research. 2023; 30(4):9184-206. https://doi.org/10.1007/s11356-022-24440-4
21. Das B, Singh S, Thakur P, Jain SK. Assessment of future groundwater levels using Visual MODFLOW in the Gomti River basin in India: Theoretical and Applied Climatology. 2024; 155(4):2917-36. https://doi.org/10.1007/s00704-023-04795-5
22. Rumynin VG, Leskova PG, Sindalovskiy LN, Nikulenkov AM. Effect of depth-dependent hydraulic conductivity and anisotropy on transit time distributions. Journal of Hydrology. 2019; 579:124161. https://doi.org/10.1016/j.jhydrol.2019.124161
23. Jing M, Lu C, Heße F, Kumar R. A novel analytical model for the transit time distributions in urban groundwater systems. Journal of Hydrology. 2022; 605:127379. https://doi.org/10.1016/j.jhydrol.2021.127379
24. Bruggeman GA. Analytical solutions of geohydrological problems. Elsevier. 1999.
25. Rousseau M, Pabst T. Analytical solution and numerical simulation of steady flow around a circular heterogeneity with anisotropic and concentrically varying permeability. Water Resources Research. 2021; 57(11): e2021WR029978. https://doi.org/10.1029/2021WR029978
26. Mahdavi A. Steady-state response of annular wedge-shaped aquifers to arbitrarily-located multiwells with regional flow. Journal of Hydrology. 2020; 586:124906. https://doi.org/10.1016/j.jhydrol.2020.124906
27. Mahdavi A. Response of dual-zone heterogeneous wedge-shaped aquifers under steady-state pumping and regional flow. Advances in Water Resources. 2021;147:103823. https://doi.org/10.1016/j.advwatres.2020.103823
28. Kacimov AR, Obnosov YV. Well-bore clogging of a pumping well in hydraulic interference with an ambient groundwater flow: the Strack-Kostitsina refraction problem in an annular composite redux. Hydrogeology Journal. 2018; 26(7):2531-2541. https://doi.org/10.1007/s10040-018-1857-4
29. Strack ODL. Analytical groundwater mechanics. Cambridge University Press. 2017.
30. Lin YC, Yang SY, Fen CS, Yeh HD. A general analytical model for pumping tests in radial finite two-zone confined aquifers with Robin-type outer boundary. Journal of Hydrology. 2016; 540:1162-75. https://doi.org/10.1016/j.jhydrol.2016.07.028
31. Lin JH, Lin YF. Theoretical evaluation of high-permeability wellbore skin effect on aquifer response under pumping. Journal of Hydrology. 2024;641:131824. https://doi.org/10.1016/j.jhydrol.2024.131824
32. Chesnaux R, Molson JU, Chapuis RP. An analytical solution for ground water transit time through unconfined aquifers. Groundwater. 2005;43(4):511-517. https://doi.org/10.1111/j.1745-6584.2005.0056.x
33. Frampton A. Flow channelling and variability in transit times and tortuosity in a fractured rock model with small scale heterogeneity. Advances in Geosciences. 2025;65:149-158. https://doi.org/10.5194/adgeo-65-149-2025
34. Hayek M. Steady-state flow under surface recharge through unconfined aquifer with depth-decaying hydraulic conductivity: Analytical results. Journal of Hydrology. 2024;638:131469. https://doi.org/10.1016/j.jhydrol.2024.131469

Appendix A

When the wellbore boundary condition, Eq. (2), is imposed on the general solution, Eq. (9), the following relationships are derived:

$$A_{1,0} = 1 \tag{A1}$$

$$A_{1,1} + B_{1,1} = 0 \tag{A2}$$

To satisfy Eq. (3), which ensures the continuity of drawdown at the skin-formation interface, the following conditions must hold:

$$A_{1,0} + B_{1,0} \ln r_{s,D} = A_{2,0} + B_{2,0} \ln r_{s,D} \tag{A3}$$

$$A_{1,1} r_{s,D} + \frac{B_{1,1}}{r_{s,D}} = A_{21} r_{s,D} + \frac{B_{2,1}}{r_{s,D}} \tag{A4}$$

The continuity of flux at the skin-formation interface, as described by Eq. (4), yields:

$$B_{1,0} = \kappa B_{2,0} \tag{A5}$$

$$A_{1,1} - \frac{B_{1,1}}{r_{s,D}^2} = \kappa \left(A_{2,1} - \frac{B_{2,1}}{r_{s,D}^2} \right) \tag{A6}$$

Finally, the remote boundary condition, Eq. (7), results in:

$$A_{2,0} + B_{2,0} \ln R_D = 0 \tag{A7}$$

$$A_{2,1} R_D + \frac{B_{2,1}}{R_D} = U_D R_D \tag{A8}$$

Equations (A1)-(A8) form a set of eight linearly independent equations, with the solution presented in Table 1.

Table 1: Lumped parameters appearing in the formulation (dimensionless)

$$A_{1,1} = \frac{2U_D \kappa}{F}$$

$$A_{2,0} = -\frac{\ln R_D}{E}$$

$$A_{2,1} = \frac{U_D}{F}\left[\frac{1-\kappa}{r_{s,D}^2} + \kappa + 1\right]$$

$$B_{1,0} = \frac{\kappa}{E}$$

$$B_{1,1} = -\frac{2U_D \kappa}{F}$$

$$B_{2,0} = \frac{1}{E}$$

$$B_{2,1} = \frac{U_D}{F}\left[(\kappa - 1) r_{s,D}^2 - \kappa - 1\right]$$

$$E = \ln \frac{r_{s,D}^{1-\kappa}}{R_D}$$

$$F = (1-\kappa)\left[\frac{1}{r_{s,D}^2} - \left(\frac{r_{s,D}}{R_D}\right)^2\right] + (1+\kappa)\left[1 - \frac{1}{R_D^2}\right]$$

Table 2: Monitoring-well locations and corresponding observed and calculated drawdowns.

Well number	Well's radial coordinate, r_D	Well's angular coordinate, θ	Observed drawdown	Calculated drawdown
1	60	0	0.2865	0.2824
2	80	π/2	0.2378	0.2665
3	120	π	0.2567	0.2440
4	180	π/6	0.2372	0.2219
5	250	5π/6	0.2072	0.2034
6	350	3π/2	0.1914	0.1850
7	500	π/3	0.1708	0.1656
8	700	π	0.1406	0.1461
9	950	5π/3	0.1322	0.1304
10	1300	0	0.1047	0.1139
11	1800	2π/3	0.0960	0.0937
12	2500	4π/3	0.0638	0.0752
13	3300	π/6	0.0573	0.0641
14	4300	5π/6	0.0387	0.0428
15	5500	3π/2	0.0346	0.0330
16	6800	π/3	0.0253	0.0247
17	8000	4π/3	0.0078	0.0083
18	9000	5π/6	-0.0023	-0.0021
19	9800	11π/6	0.0087	0.0097

© 2026 by the authors. Licensee SCU, Ahvaz, Iran. This article is an open access article distributed under the terms and conditions of the Creative Commons Attribution 4.0 International (CC BY 4.0 license) (http://creativecommons.org/licenses/by/4.0/).